PCCP

ARTICLE TYPE

Cite this: DOI: 00.0000/xxxxxxxxxx

Coalescence of AuPd nanoalloys in implicit environments†

Sofia Zinzani,[a] Francesca Baletto[a‡]

Received Date
Accepted Date

DOI: 00.0000/xxxxxxxxxx

The optimal design of nanoparticles and nanoalloys arises from the control of their morphology which depends on the synthesis process they undergo. Coalescence is widely accepted as one of the most common synthetic mechanisms, and it occurs both in the liquid and gas phase. Coalescence is when two existing seeds collide and aggregate into a larger object. The resulting aggregate is expected to be far from the equilibrium isomer, i.e. the global minimum of the potential energy surface. While the coalescence of nanoparticles is well studied in the vacuum, sparse computational studies are available for the coalescence in an environment. By Molecular Dynamics simulations we study the coalescence of Au and Pd nanoseeds surrounded by an interacting environment. Comparing the initial stages of the coalescence in the vacuum and the presence of an interacting environment, we show that the kinetics of the formation process, strongly depends on the environment and on the size of the nanoalloy. Furthermore, we show that is possible to tune the resulting nanoalloys surface chemical composition by changing their surrounding environment.

1 Introduction

Since Granqvist's work and the Japanese project Erato[1], the interest in nanoparticles (NPs) remains high as they have several technological applications. To cite a few, they are the building blocks of sensors, energy harvesting devices, catalysts, and random-assembled neuromorphic systems[2–9]. A NPs is a discrete object having its three dimensions below 100 nm, and showing peculiar properties depending on its morphology. Among NPs, metallic nanoalloys (NAs) - referring to NPs made of two or more metals - possess unique chemophysical features[10–13]. We use the term architecture of a NP to combine the NAs morphology, size, shape, chemical composition, and chemical ordering of the inner and surface layer[14,15]. At the core of a rational design process, we must understand how NAs form, evolve, and agglomerate. Numerical methods can shed light on the atomistic processes and the kinetics of the formation/agglomeration processes providing complementary information to experimental techniques[16–18]. Generally speaking, the formation of NPs and NAs follows three possible paths: (i) By the subsequent deposition of atoms over an existing core -the so-called one-by-one growth[19]; (ii) By the coalescence - the sintering of two or more individual seeds; (iii) Annealing of a melted seed with a certain rate[20]. During the coalescence and the one-by-one growth processes, surface rearrangements are mainly driven by atoms diffusion and formation of small island. Annealing might be driven by pressure effects and minimisation of the surface energy contribution. Among the three growth modes, coalescence is thought to play a non-negligible role in both gas aggregation cluster sources as well as in liquid laser ablation. The latter is acquiring increasing importance in the large scale production of Au-based NAs[21]. On the modelling of coalescence, we appreciate considerably efforts in understanding the coalescence of Au-based NAs[22–25]. Nonetheless, at our knowledge, those studies refers to the coalescence in the perfect vacuum although likely the surroundings may affect both NA stability, i.e. surface energy, and kinetics, i.e. atoms diffusion. Our interest is in understanding the effect of an environment around NAs during their formation process. We focus on Au-Pd NAs because of their role in heterogeneous thermal catalysis and electrocatalysis, as they exhibit superior activity and enhanced selectivity[26–29]. The rationale for combining Au with Pd is due to the plasmonic and versatile character of Au-seed with the strong catalytic flavour of the Pd. Nano Au-Pd is employed in industrial processes such as hydrogen peroxide synthesis from H_2 and O_2, alcohol oxidation[30], vinyl acetate monomer synthesis[31], and formic acid de-hydrogenation[32].

Several studies report the complex energy landscape of Au-Pd.[33,34]. They show a tendency to form Au-rich surfaces, with ball (Pd)-cup (Au) chemical ordering predicted at sizes up to 3 nm[35]. We investigate and compare the kinetics of the coales-

[a] *Università degli Studi di Milano - Dipartimento di Fisica; Via Celoria 16; Milano I-20133; Italy.*

‡ *E-mail: francesca.baletto@unimi.it*

† Electronic Supplementary Information (ESI) available: [MEIs selected, Supplementary characterization methods: PDDF in Sapphire, Au_{55}^{Ih}-Pd_{55}^{Ih}, Au_{561}^{Ih}-Pd_{561}^{Ih}]. See DOI: 10.1039/cXCP00000x/

cence of a gold and a palladium seeds over a few tens of ns both in the vacuum and in a plethora of environments. We use the Huerto-Cortes' formalism[36] to mimic a uniform medium around the NA and we can tune the type and the strength of the interaction for each chemical species. We reveal that the surface chemical composition and the timescale of the sintering process depend significantly on the environment.

2 Methodology

We study the first steps of the coalescence of a 55-atom gold icosahedron (Ih), Au_{55}^{Ih}, against a 55-atom Ih of palladium, Pd_{55}^{Ih}, leading to a $AuPd_{110}$. We, then, consider the coalescence of a Au_{561}^{Ih} against a Pd_{561}^{Ih}. In Figure 1 we report a pictorial representation of the coalescence process.

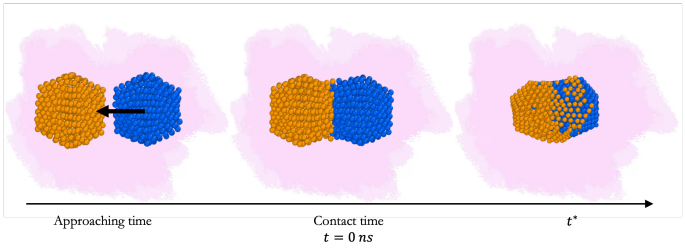

Fig. 1 Pictorial image for the coalescence. In pink is represented the implicit interacting environment. In orange and blue respectively the Au and Pd atoms of two NPs. Along the axis we report the time evolution of the coalescence process: it starts with the approaching time, we named *contact time* the instant when the two NPs touch each other and in the main text this is considered the time corresponding to 0 ns. Then the coalescence continues, and we represent with t^* a generic instant after the contact time.

To understand the effect of the medium, we vary the strength and the type of interaction between metal atoms and environment (metal-environment interaction, `MEI`).

We keep the chemical composition equal to 50%, and select the same initial geometrical shape, namely an icosahedron, for both seed. The rational behind our choice is that often noble and quasi-noble clusters in the 1-3 nm size-range shapes as an Ih which is the closest structure to a sphere.[16]

We perform classical molecular dynamics simulations, using the open-source package `LoDiS`[37]. An Andersen thermostat with a frequency of 10^{11}Hz controls the temperature of each run. We choose 400K for the coalescence of Au_{55}^{Ih} - Pd_{55}^{Ih} and 600 K for the Au_{561}^{Ih} - Pd_{561}^{Ih}. This because we note that at 600 K, the gold region in any $AuPd_{110}$ almost melts leading to more mixed and structurally disordered NA independently of the metal-environment interaction. As we want to address the effect of the environment before melting occurs, we do not comment this case further. Because we are interested in the first stages of the formation process, the trajectories are collect over 10-20 ns after the two seeds comes in contact, sampling the geometrical a configurations each 0.01 ns. Preliminary simulations over 100 ns show that major structural changes occur in a period of 10-20 ns. We average our results over four independent simulations.

The metal-metal interaction is modelled according to the second moment approximation (SMA) in the tight-binding (TB) model[38], which is widely used to mimic the growth of NPs and NAs[39–41]. In such framework, the total energy of each atom i contains an attractive many-body term and a 2-body repulsive term, as

$$E^i_{TBSMA}(r_{ij}) = \sum_{j\neq i}^{n_v} A_{ab} e^{-p_{ab}\left(\frac{r_{ij}}{r^0_{ab}}-1\right)} - \sqrt{\sum_{j\neq i}^{n_v} \xi^2_{ab} e^{-2q_{ab}\left(\frac{r_{ij}}{r^0_{ab}}-1\right)}} \quad ,$$

where r^0_{ab} is the lattice parameter of individual chemical species, or their arithmetic mean for hetero-pairs; r_{ij} is the atomic pair distances; n_v is the number of neighbours falling within a radius between the bulk second and third neighbour distances. The parameters A_{ab}, ξ_{ab}, p_{ab}, and q_{ab} are determined to reproduce the experimental values of the cohesive energy, elastic constant, lattice parameter and bulk modulus. Table 2 summarises the TB-SMA parameters used for the gold-palladium system[42].

	p	q	A [eV]	ξ [eV]
Au-Au	10.139	4.033	0.2095	1.8153
Pd-Pd	11.0	3.794	0.1715	1.7019
Au-Pd	10.543	3.8862	0.1897	1.7536

We model the metal-environment interaction (MEI), E^{M-E} via the Huerto-Cortes, Goniakowski, Noguera's formalism[36] . The contribution of the atom i of chemical type α, $E^{M-E}_{i\in\alpha}$, depends on the number of unsaturated bonds with respect to the bulk, namely the difference between the maximum (bulk) and the atomic coordination number $CN_{i\in\alpha}$,

$$E^{M-E}_{i\in\alpha} = -\eta_\alpha (CN_{bulk} - CN_{i\in\alpha})^{\rho_\alpha} \quad . \tag{1}$$

We set CN_{bulk} to 12 as both Au and Pd are FCC metals in the bulk. The strength of the interaction is tuned by η_α while ρ_α controls the type of interaction. For example, $\rho = 1$ stands for a pairwise interaction; while covalent interaction occurs when $\rho < 1$ and $\rho > 1$ is for strongly-interacting environments[36].

For the AuPd NAs, we vary the four parameters ρ_{Au}, ρ_{Pd}, η_{Au}, η_{Pd} and we identify 37 MEIs listed in Table S1 of Supplementary Information. The choice of our η and ρ has been made exploring different type of interactions, and considering an estimate of the surface energy of a plane p $\gamma_p \sim k_\alpha (CB_{bulk} - CN^p)\left[1 - \frac{\eta_\alpha}{k_\alpha}(CB_{bulk} - CN^p)^{(\rho-1)}\right]$, based on what reported by Huerto-Cortes et al.[36],[43]. The considered MEIs should not alter the relative stability of surface energy, but might equally favour the presence of Pd at the surface.

We split MEIs into three groups:

- MEI-A: only Au atoms interact with the environment, setting $\eta_{Pd} = 0$ eV. ρ_{Au} is 0.5, 1.0, 1.5 and η_{Au} between 0.02 and 0.08 eV, respectively.
- MEI-P: only Pd atoms interact with the environment, $\eta_{Au} = 0$ eV. ρ_{Pd} is 0.5, 1.0, 1.5 and η_{Pd} equals to 0.02 eV, 0.08 eV. In Suppl. Info. we show results with $\eta_{Pd} = 0.2$ eV, and for (0.06 eV; 1.5).
- MEI-AP: both Au and Pd interacting. We fix the Au values to (0.02 eV, 0.5) while Pd-E interactions are with ρ_{Pd} equals

0.5, 0.75, 1.0, 1.5 and $\eta_{Pd} = 0.02$, 0.04 , 0.06 , 0.08, and 0.2 eV.

For the coalescence of Au_{561}^{Ih} - Pd_{561}^{Ih} we select fewer MEIs among group P and AP: (i) P-group: $\rho_{Pd} = 1.5$ and $\eta_{Pd} = 0.08$ eV; (ii) AP: ρ_{Pd} is 0.5, 1.0, 1.5 and $\eta_{Pd} = 0.02$ eV, and 0.08 eV. Such reduction is motivated by the results obtained on the 110 atoms system and to save computational time. In the main text, we discuss four cases, namely the vacuum, a MEI-AP, a MEI-P and a MEI-A. All the results from other environments are available in Suppl. Info.

2.1 Characterisation tools

We analyse and characterise the classical MD trajectories using the `Sapphire` suite[44]. We select a few descriptors to quantify the structural and chemical changes during the coalescence of AuPd. Our aim is to show the effect of the environment on the kinetics of the coalescence and on the surface chemical ordering. We focus on the evolution of the neck region, i.e., the spatial region where the coalecence occurs, the MEI effect on NA shrinking and on any significant change in the surface chemical composition. We do not report any structural classification of the resulting NAs, but we have calculated common neighbour analysis signatures and patterns.

Layer-by-layer analysis We perform a layer-by-layer (LBL) analysis in the direction perpendicular to the coalescence axis, defined as the axis where the center of mass of the individual seed lies on. The analysis code is available at `Sapphirine`, the version 2.0 of the `Sapphire` code. First a rotation of all atomic coordinates is applied to align the coalescence axis along a Cartesian axis, e.g. z-axis. Then the NP is sliced into layers and binned in 2.25 Å, about the inter-layer distance of (111) planes in a Pd bulk. We monitor the number of layer versus time, $m_l(t)$, and we count the number of atoms per each chemical species α in each layer, $N_l^{\alpha}(t)$. The neck is the poorly populated region between the two initial seeds. It is expected when the total number of atoms per layer, $N_l(t) = N_l^{Au}(t) + N_l^{Pd}(t)$, has a non-monotonic behaviour with respect the layering. A neck is still present until the minimum of $N_l(t)$ falls within an intermediate position between the two centers of mass and it is lower than the expected number of atoms per layer, $N_l^{expected}$. Assuming an uniform distribution of atoms in the NA, $N_l^{expected}(t) = \frac{N}{m_l(t)}$ where N is the total number of atoms and $m_l(t)$ is the number of layers at that time. If $N_l(t)$ crosses $N_l^{expected}(t)$ more than twice, we conclude that a neck is still present, as visible from Figure 2. We define the *neck life-time* (LTN) as the first instant since $N_l^{expected}(t)$ is crossed only twice.

Chemical ordering To analyse on-the-fly the chemical ordering in the NA we use various descriptors. To characterize the local environment of an atom we start counting the number of its nearest neighbours: we consider a cut-off region, described by a sphere with radius equal to the bulk nearest neighbour distance and centered around the atom, and enumerate the other atoms that fall in such region. Starting from this quantity we are able to calculate

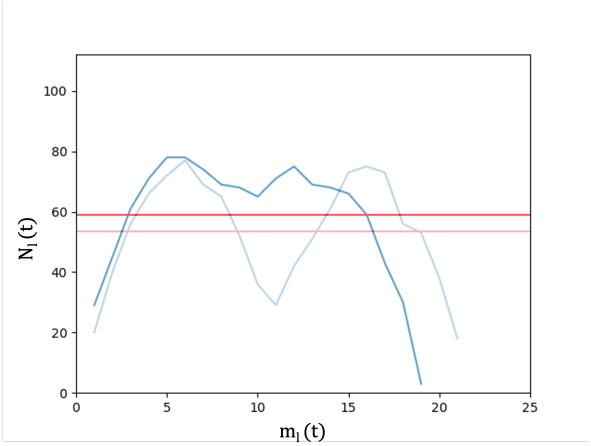

Fig. 2 LBL analysis during the coalescence of Au_{561}^{Ih}-Pd_{561}^{Ih} in the vacuum. The straight light red and red lines are the $N_l^{expected}(t)$ values at the beginning and after 0.07 ns, respectively. The profile of the layer population $N_l(t=0)$ and $N_l(t=0.07ns)$ are in light blue and in blue, respectively. $N_l(t=0)$ shows a neck corresponding at the depression below its $N_l^{expected}$. After 0.07 ns, the distribution profile N_l shows an almost flat distribution in the middle region with the neck disappearing.

the mixing parameter $\mu(t)$,

$$\mu(t) = \frac{\sum_\alpha CN_\alpha^{homo}(t) - CN_{hetero}(t)}{\sum_\alpha CN_\alpha^{homo}(t) + CN_{hetero}(t)}. \quad (2)$$

as widely used in the literature[10]. $\mu(t)$ is the ration between the number of nearest-neighbour homo-pairs $CN_{\alpha\alpha}^{homo}$, and the total number of nearest-neighbour hetero-pairs $CN_{\alpha\beta}^{hetero}$, per each configuration at time t. $\mu(t)$ ranges between [-1;1] where -1 is for a fully alloyed, and $+1$ a complete phase separated system.

Counting homo and hetero pairs follows the introduction of a cut-off distance, R_{cut}, as the first minimum of the pair-distance distribution function, PDDF, as in `Sapphire`. From that cutoff we build the the adjacency matrix, $A(r_{ij})$. $A(r_{ij})$ is set to 1 if the distance between atoms is less than the R_{cut} and 0 if it is greater. The atomic coordination number CN_i, is then the sum over a row/column of $A(r_{ij})$

$$\begin{aligned} CN_i &= \sum_{j \neq i} A\left(r_{ij}\right) \\ CN_{\alpha\alpha}^{homo} &= \sum_{i,j \in \alpha,\ i \neq j} A\left(r_{ij}\right) \\ CN_{\alpha\beta}^{hetero} &= \sum_{i \in \alpha,\ j \in \beta} A\left(r_{ij}\right) \end{aligned} \quad , \quad (3)$$

where α, β label two different chemical species. The PDDF is a crucial quantity to characterise the geometry of a NP, not only because it enables to define a R_{cut} but also because a second peak the PDDF in correspondence of the bulk lattice parameter (a_0) stems for a geometrical order[45]. We note that The maximum of the PDDF, D_{max}, provides an estimate of the NP size.

The local atomic environment (LAE) counts the total number of hetero-bonds the atom i forms. LAE $= 0$ indicates that there are no hetero-bonds; $1 \geq$ LAE ≤ 6 shows a mild mixing tendency.

Finally, LAE ≥ 9 indicates that β-atoms are encapsulated into a α-matrix. Counting the occurrence of each LAE provides a clear representation of the overall chemical of the NA. For example, a core-shell nanoalloy with a one layer thick shell of α-atoms is characterised by a negligible value of $\text{LAE}_\alpha = 0$ but an high occurrence of 1 <= LAE <= 6, for both chemical species.

We evaluate the chemical radius of gyration R^α_{gyr}, the radius of gyration referred to each chemical species. R^α_{gyr} quantifies by which extent atoms are spread around their centre of mass (CoM_w);

$$R^\alpha_{gyr} = \sqrt{\frac{1}{N_\alpha}\sum_{i\in\alpha}^{N}(r_i - \text{CoM}_\alpha)^2} \quad , \tag{4}$$

where α is either gold or palladium, N_α is the total number of atoms of that chemical specie, CoM_α is the centre if mass of N_α only. Chemical radius of gyration, combined with the distance between the center of mass of the Au and Pd regions, ΔCoM, provides an indication of the chemical ordering. For example, the condition $R^{Au}_{gyr} \sim R^{Pd}_{gyr}$ and $CoM_{Au} \sim CoM_{Pd}$ occurs only in a mixed alloyed system. On the other hand, $CoM_{Au} \sim CoM_{Pd}$ but $R^{Au}_{gyr} > R^{Pd}_{gyr}$ stands for a core-shell with Au-rich external shell.

Surface identification We identify surface atoms when its atop generalized coordination number is less than 10, as implemented in `Sapphire`[44]. Let $N^S_A(t)$ and $N^S_B(t)$ be the number of surface atoms of type A and B. Obviously, the total number of surface atoms is simply the sum of the two contribution, $N^S(t) = N^S_A(t) + N^S_B(t)$. The *absolute percentage* of α-atoms at the surface is the ratio between $P_{\alpha_S,abs} = \frac{N^S_\alpha}{N^S_{tot}}$. In Suppl. Info., we provide the behaviour of the *relative percentage* $P_{\alpha_S,rel}$, defined as the percentage of atoms of a given type with respect to its total number.

3 Results

Let us to compare the initial stages of the coalescence in the vacuum and with a certain MEI, elucidating how the neck dynamics is affected and the remaining into an elongated shape against a more spherical one, i.e., *shrinking process*. Top row of Fig. 3 shows the evolution of the number of layers, $m_l(t)$, and their population, namely the number of atoms per each layer, $N^(_l t)$, for a typical run for Au^{Ih}_{55}-Pd^{Ih}_{55} and Au^{Ih}_{561}-Pd^{Ih}_{561}. Time is set to zero when the two seed collides and the layers are counted from the Pd-seed. Clearly, $m_l(t)$ decreases with time and the effect is stronger at small sizes, where in just a few frames $m_l(t)$ almost halves. On the other hand, at 1122 atoms only few layers are lost over 20 ns. The resulting shape is still elongated with a peak of the most populated layers located in the Pd region. In any event, we observe a smooth behaviour of the population per layer.

The neck lifetime, LTN, middle row of 3, averages at 0.02 ns and always less than 0.06 ns for 110 atoms, while it ranges between 0.05 and 0.2 ns for 1122 atoms. At Au^{Ih}_{561}-Pd^{Ih}_{561}, a mild effect due to the environment occurs with respect to the vacuum. A few MEIs, `set24, set34, set134`, increase the LTN but others, `set1, set3`, fasten it. See Suppl. Info. for details on those MEIs.

To further characterise the shrinking process, we compare the difference between the number of layer for a certain MEI, $m_l(t)^{MEI}$, and the same quantity in the vacuum, $m_l(t)^v$, $\Delta_{layers} = m_l(t)^{MEI} - m_l(t)^v$, shown in Figure 3 at the start (gray circles) of the coalescence and after 10 ns for Au^{Ih}_{55}-Pd^{Ih}_{55} and 20 ns for Au^{Ih}_{561}-Pd^{Ih}_{561} (black stars). We note that the environment barely influences when the two seeds come in contact, suggesting that our choice of the MEI affects mainly the surface diffusion and hence the dynamics of the *shrinking process*.

The dynamics of the aggregation of Au^{Ih}_{55} and Pd^{Ih}_{55} remains almost unchanged, with Δ_{layers} less than half of a layer. On the other hand, the shrinking process of Au^{Ih}_{561}-Pd^{Ih}_{561} depends on the surrounding and it can be either fasten up or slowed down. The interaction between Pd atoms and the environment turns to be the key factor, while the Au-environment interaction poorly affects the process. If Pd is strongly interacting, e.g. `set34, set134`, it is more likely to observe elongated shapes. While if Pd interacts weakly ($\rho = 0.5$, `set1, set2, set3, set4`), the shape of the NA is more compact than in the vacuum already after 20 ns.

To investigate whether the chemical ordering and the surface composition is affected by the MEI, we compare various descriptors. Figs. 4 and 5 show the behaviour at 110 and 1122 atoms, respectively, in the vacuum and within the `set34`, a MEI-AP with Pd strongly interacting and Au weakly.

First, the chemical R^α_{gyr} are noisy, mainly for Au, and both chemical species expands after the collision. In the vacuum, the Pd-spreading is little and at small sizes the chemical radii of gyration overlaps in the MEI-AP. The $R^{Pd}_{gyr} \sim R^{Au}_{gyr}$ if not even bigger suggest Pd atoms populate the external layer. For Au^{Ih}_{561} - Pd^{Ih}_{561}, R^{Pd}_{gyr} evolves at the same pace of R^{Au}_{gyr}, indicating that both chemical species are diffusing at the surface, while it was almost constant in the vacuum. The behaviour of R^{Pd}_{gyr} together with the drop of ΔCoM suggests the presence of a partial core-shell chemical ordering in the AuPd in the vacuum, while we expect an intermixed surface layer in the MEI-AP.

Such picture is confirmed by the relative abundance of surface atoms, see bottom rows of Figures 4 and 5. For the coalescence in the vacuum, the surface is mainly composed by Au atoms. Introducing a strongly interacting environment with Pd only, this chemical species tends to be at the surface, occupying about 50% of the surface area, Figure 4, and a $\mu(t)$ of just 0.4, much less than the 0.6 in the vacuum. The more we decrease the values of ρ and η, the more the μ tends to its value in the vacuum. This suggests that mildly interacting environments, both in terms of the type of interaction and the strength of the interaction, will affect poorly the dynamics of aggregation and the overall chemical stability of NAs. At larger sizes, the MEI affects the chemical ordering although less pronounced. We believe this is only a kinetic effect as shown by a more elongated shape. Full details of the $\mu(t)$ analysis are reported in Suppl. Info. but they do confirm a tendency to mix in the considered MEI-AP.

At 110 atoms, for `set0` or the vacuum, we observe a predominance of ball-cup chemical ordering, where the Pd region is only partially covered by a Au-monolayer. To be more quantitative, we analyse the local atomic environment (LAE) for each chemical species, see Fig. 6. For $Au^{Ih}_{55}Pd^{Ih}_{55}$ after 10 ns in the vacuum,

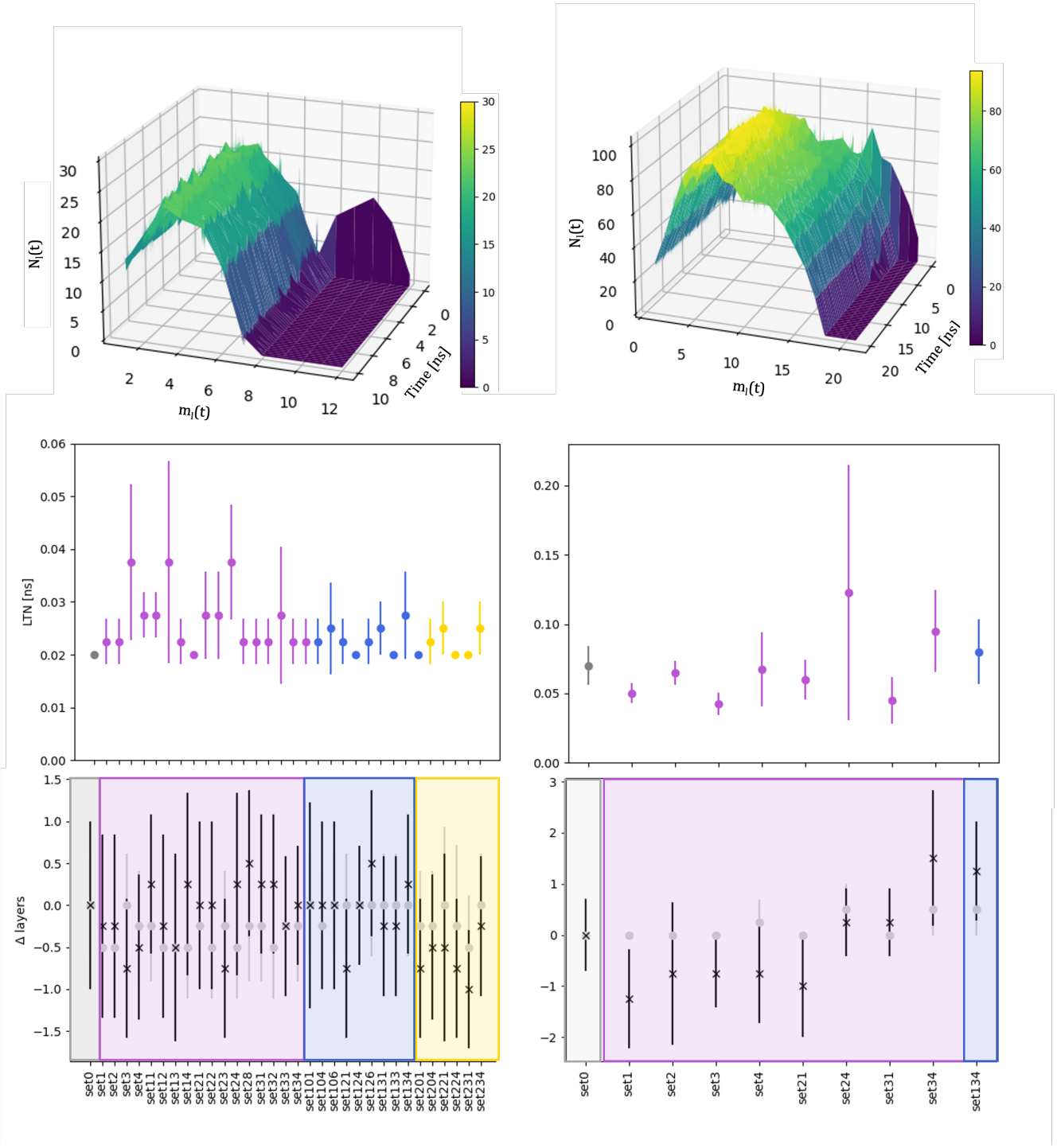

Fig. 3 Left column refers to Au^{Ih}_{55}-Pd^{Ih}_{55} and right column to Au^{Ih}_{561}-Pd^{Ih}_{561} Top: Distribution of the number of atoms per layer with $\rho_{Au} = 0.5$, $\rho_{Pd} = 1.5$, $\eta_{Au} = 0.02$ eV and $\eta_{Pd} = 0.8$ eV, aka set34. The colour gradient represents $N_l(t)$. Middle: mean value of the LTN and its standard deviation over independent simulations for each MEI. Vacuum, labelled as set0 is in gray. Bottom: difference between the number of layers $N_l(t)$ in a MEI and in the vacuum (Δ_{layers}) averaged over the independent simulations and their standard deviation, at the initial time (gray full circles) and after 10 ns for Au^{Ih}_{55}-Pd^{Ih}_{55} and 20 ns for Au^{Ih}_{561}-Pd^{Ih}_{561} (black stars). For middle and bottom rows, the x-axis labels the environment, MEIs are coloured in accordance to with chemical species interacts: only Pd in blue (MEI-P); only Au in yellow (MEI-A); both Au and Pd interacting (MEI-AP) are in violet. For a full description of the MEI see table S1 of Suppl. Info.

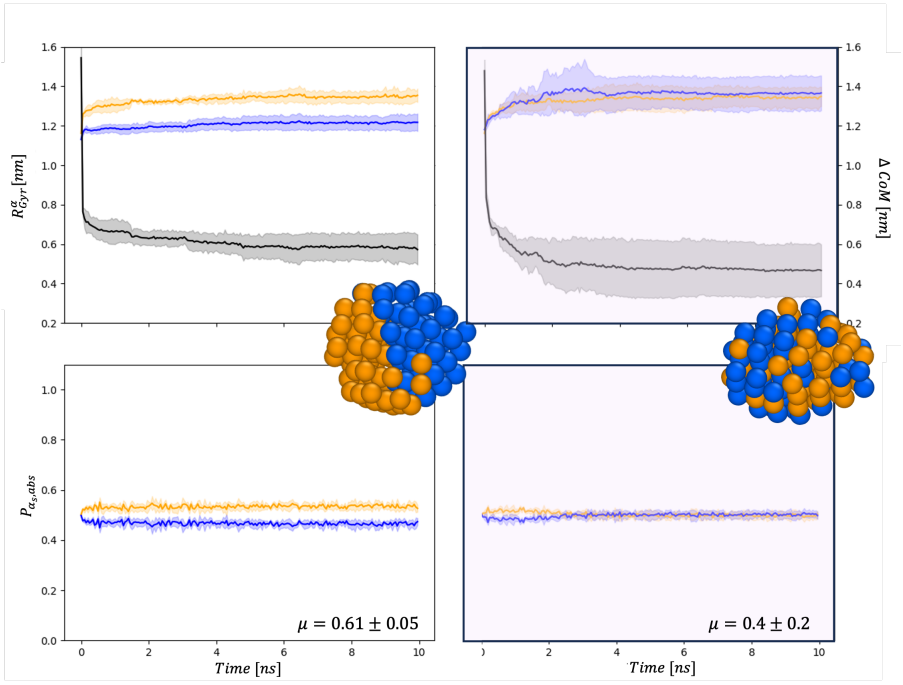

Fig. 4 Chemical distribution in Au^{Ih}_{55}-Pd^{Ih}_{55} in the vacuum (left) and in set34 (right). Paradigmatic snapshots taken after 10 ns where Au atoms are orange, and Pd in blue. Top panel: Referring on the left y-axis: time evolution of R^{α}_{gyr} in nm. Solid line is the averaged value over the independent simulations, Au in orange and Pd in blue, respectively. The shadow represents their standard deviation. In black the time evolution distance between the centers of mass of the two chemical species ΔCoM, referring on the right axis. Bottom panel: Time evolution of the percentage of surface atoms of type α with respect to the number of surface atoms, $P_{\alpha,abs}$. Colour as in the above panels. Also the μ at 10 ns averaged over the 4 independent simulations, with its standard deviation is reported in these figures.

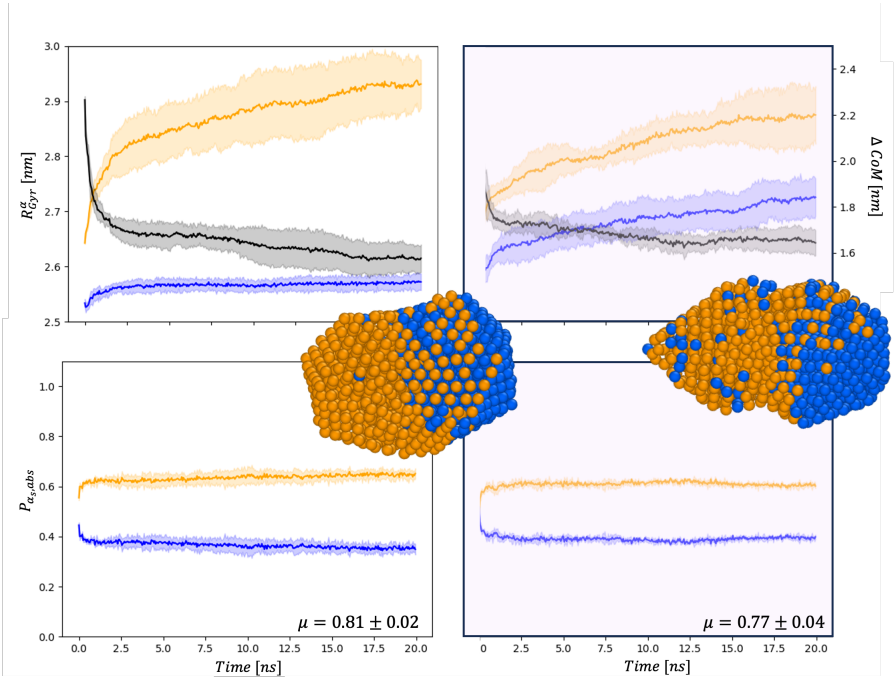

Fig. 5 Chemical distribution for Au^{Ih}_{561}-Pd^{Ih}_{561} in the vacuum (right) and and in set34 (right) for R^{α}_{gyr} in nm and ΔCoM in nm (top), and $P_{\alpha,abs}$ (bottom). Snapshots taken after 20 ns same colour coding as in Fig. 4.

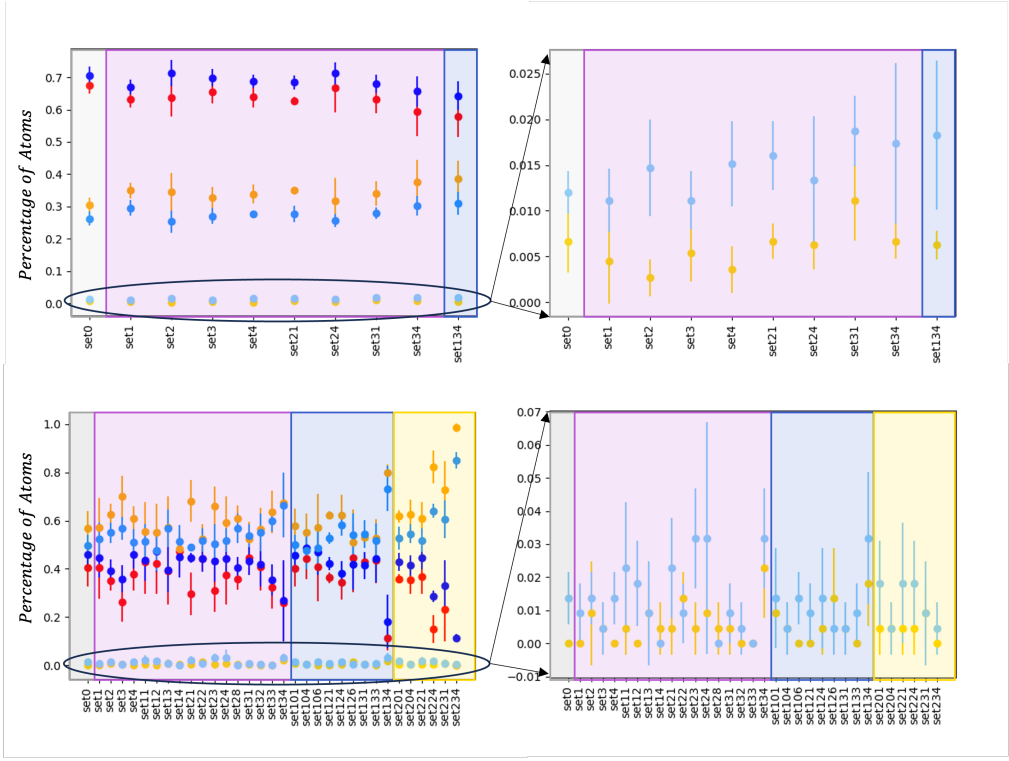

Fig. 6 Percentage of the three LAEs defined in the text, for each chemical species, referred to the last configuration and averaged over all independent simulations for Au^{Ih}_{561}-Pd^{Ih}_{561} (top) and Au^{Ih}_{55}-Pd^{Ih}_{55} (bottom). Chemical local environment for Au are $\text{LAE}_{Au}=0$ in red, $\text{LAE}_{Au}\in(3-6)$ in orange, ≥ 9 in yellow. While Pd chemical LAE are in blue, light-blue, sky, respectively. The right column is a zoom of the situation with a LAE ≥ 9.

$\text{LAE}_{Au}=0\sim 40\%$ <$\text{LAE}_{Au}\in(3-6)\sim 55\%$ and $\text{LAE}_{Pd}=0\sim\text{LAE}_{Pd}\in(3-6)\sim 45\%$, while there is a negligible occurrence of Au and Pd atoms in a fully mixed local environment (LAE $\geq$ 9). We note that LAE_{Au}=0 is always less or equal than LAE_{Pd}=0 supporting the idea that Au atoms diffuse over Pd. Furthermore, a feature of LAE_{Pd}=0 about 50% suggests that the Pd-seed is at least partially preserved. At the same time, but in a few cases, we observe individual Pd atoms embedded in a Au-matrix ($\text{LAE}_{Pd}\geq$9, see zoomed panel of 6). For example, `set34, set134, set 124, set224, set 231, set 234` suggest a different chemical ordering than the vacuum highlighted by a drop of each LAE=0 together with an increment of the LAE$\in(3-6)$. In particular, the LAE signatures for `set234`, namely LAE=0 and LAE$\geq$9 both lower than 10% and LAE$\in(3-6)$ above 80% for both chemical species suggest the formation of a Au-shell over a Pd-core. On the other hand, `set34, set134`, with Pd strongly interacting, predict a stronger mixing with some Pd atoms dispersed in the Au matrix, and a low LAE=0 and a high LAE$\in(3-6)$ for both chemical species.

At 1122, again the effect of the MEI seems less evident because of the simulation time relatively shorter than at the 110 atoms. Nonetheless, there is a clear indication that `set34, set134` behave differently than the vacuum. In particular, the $\text{LAE}_{Pd}\geq$9 are almost 2% and there is a trend to increase the mixing both at the surface and in the inner.

For both sizes and all the MEIs, a greater structural order emerges at the end of the simulation (10ns for Au^{Ih}_{55} - Pd^{Ih}_{55} and 20ns for Au^{Ih}_{561} - Pd^{Ih}_{561}) with respect to the time zero, set as the contact time of the two seeds, see PDDFs profiles in Figs. S4, S5, S6, S27, S28. A deeper look indicates that the Pd region displays a geometrical order, even at small sizes while the PDDF of the Au-part does not often show a peak at the lattice distance, Figs. S7, S8, S9. In any event, the distance between the two seeds is similar and tend to be close to 1.6 .

For Au^{Ih}_{561} - Pd^{Ih}_{561} in the vacuum, the Pd-region tends to remain as the original icosahedral seed, with few Au atoms hopping over its surface. On the contrary, in presence of a strong MEI-P or a MEI-AP, an intermixing of Pd and Au at the surface is observed. As Pd strongly interact with the surrounding, Pd atoms spread in a random way around the surface layer, eventually clustering along low coordinated sites, i.e. edges, in order to balance the interaction with the implicit environment.

4 Conclusions

Through classical Molecular Dynamics simulations, we model the coalescence of gold and palladium NPs, both in vacuum and embedded in an environment through an implicit model. We examine the coalescence of two 55-atoms seeds, simulated at 400K, and of two seeds of 561 atoms each, simulated at 600K. at both sizes, we select icosahedral seeds of same size. We tune the parameters of the interacting environment obtaining 37 different simulations systems. We study the initial steps of the coalescence process and we provide insights on the different surface chemical composition in the first 10-20 ns.

Our analysis reveals that the neck disappears in 0.06 ns for 110 atoms and 0.2 ns for 1122 atoms in all surroundings, and the environment might affect little its lifetime. The rate of shrinking

is influenced by the size of the nanoalloy and by the surrounding. Notably, when observing the process over 20 ns, certain environments induce a more compact shape compared to vacuum conditions, while others slow down the process leading to more elongated shapes than in the vacuum.

At small sizes, we observe a pronounced tendency towards the formation of ball-cup structures, in good agreement with global optimization studies[46], where the innermost layers are mainly of Pd and gold atoms diffuse above the Pd seed to form a partial external shell. Nonetheless, when Pd interacts strongly with the environment, the preferential chemical ordering changes towards a mixed nanoalloy with both Pd and Au are equally abundant at the NA surface. At large sizes, we observe that Pd tends to keep its icosahedral shape and Au diffuses upon it. In strong MEI-AP and MEI-P, we reveal the formation of a intermixed external shell, with Au diffusing over Pd atoms and a few Pd inter-diffusing in Au layers.

In conclusion, our research shows clearly that the presence of an interacting environment affects the dynamics of the coalescence process, as well as the surface chemical composition of AuPd NAs. The need to consider the environment when modeling the trajectory of NAs formation and predicting their physicochemical properties is then evident. Moreover, the kinetics of the shrinking is size and environment dependent, making not easy an extrapolation of the behaviour at other sizes or cases.

Since Au-based nanoalloys play pivotal roles in plasmonic devices and nanocatalysis, variations in environmental conditions can lead to changes and rearrangements in their morphology, thereby influencing their optical response and possibly their performance. Additionally, strongly interacting environments with the dopant transition metals, but not Au, will impact the surface chemical composition of the NAs, affecting their catalytic activity.

Availability and documentation

All the MD trajectories obtained are available on Unimi DATAVERSE[?] .

Conflicts of interest

There are no conflicts to declare.

Acknowledgements

S.Z. acknowledges the University of Milan and ISC srl for financially support her PhD studentship (D.M. 118/2023 PNRR). S.Z. thank also Dr. Mirko Vanzan for its kind support during the development of this work. Both authors acknowledge the computational resources provided by the INDACO Platform, a project of High Performance Computing at the Universitá degli Studi di Milano.

References

1 C. G. Granqvist and R. A. Buhrman, *Journal of Applied Physics*, 1976, **47**, 2200–2219.

2 V. Amendola, R. Pilot, M. Frasconi, O. M. Maragò and M. A. Iatì, *Journal of Physics: Condensed Matter*, 2017, **29**, 203002.

3 A. Longato, M. Vanzan, E. Colusso, S. Corni and A. Martucci, *Small*, 2023, **19**, 2205522.

4 Y. Yao, L. Zhang, E. Orgiu and P. Samorì, *Advanced Materials*, 2019, **31**, 1900599.

5 M. Vanzan, T. Cesca, B. Kalinic, C. Maurizio, G. Mattei and S. Corni, *ACS Photonics*, 2021, **8**, 1364–1376.

6 M. Vanzan, G. Gil, D. Castaldo, P. Nordlander and S. Corni, *Nano Letters*, 2023, **23**, 2719–2725.

7 S. Rasappa, H. Hulkkonen, L. Schulte, S. Ndoni, J. Reuna, T. Salminen and T. Niemi, *Journal of Colloid and Interface Science*, 2019, **534**, 420–429.

8 P. Jena and A. Castleman, *Nanoclusters*, Elsevier, 2010, vol. 1, pp. 1–36.

9 Z. Chai, A. Childress and A. A. Busnaina, *ACS Nano*, 2022, **16**, 17641–17686.

10 R. Ferrando, J. Jellinek and R. L. Johnston, *Chemical Reviews*, 2008, **108**, 845–910.

11 H. C. Zeng, *ChemCatChem*, 2020, **12**, 5303–5311.

12 J. Mao, J. Li, J. Pei, Y. Liu, D. Wang and Y. Li, *Nano Today*, 2019, **26**, 164–175.

13 A. Gentile, F. Ruffino and M. Grimaldi, *Nanomaterials*, 2016, **6**, 110.

14 R. L. Johnston, *Atomic and Molecular Clusters*, CRC Press Location London, 1st edn, 2002.

15 R. Kevin, *PhD thesis*, King's College London, 2019.

16 F. Baletto, *Journal of Physics: Condensed Matter*, 2019, **31**, 113001.

17 P. Grammatikopoulos, M. Sowwan and J. Kioseoglou, *Advanced Theory and Simulations*, 2019, **2**, 1900013.

18 M. Vanzan, R. M. Jones, S. Corni, R. D'Agosta and F. Baletto, *ChemPhysChem*, 2022, **23**, e202200035.

19 D. Escorcia-Díaz, S. García-Mora, L. Rendón-Castrillón, M. Ramírez-Carmona and C. Ocampo-López, *Nanomaterials*, 2023, **13**,.

20 L. Pavan, F. Baletto and R. Novakovic, *Phys. Chem. Chem. Phys.*, 2015, **17**, 28364–28371.

21 V. Amendola and M. Meneghetti, *Phys. Chem. Chem. Phys.*, 2009, **11**, 3805–3821.

22 V. Coviello, D. Forrer, P. Canton and V. Amendola, *Nanoscale*, 2024, –.

23 D. Nelli, M. Cerbelaud, R. Ferrando and C. Minnai, *Nanoscale Adv.*, 2021, **3**, 836–846.

24 V. Coviello, D. Forrer and V. Amendola, *Recent Developments in Plasmonic Alloy Nanoparticles: Synthesis, Modelling, Properties and Applications*, 2022.

25 N. Danielis, L. Vega, G. Fronzoni, M. Stener, A. Bruix and K. M. Neyman, *The Journal of Physical Chemistry C*, 2021, **125**, 17372–17384.

26 D. Astruc, *Chemical Reviews*, 2020, **120**, 461–463.

27 Z. C. C. Ozdil, O. Spalla, N. Menguy and F. Testard, *Journal of Physical Chemistry C*, 2019, **123**, 25320–25330.

28 R. Baez-Cruz, L. A. Baptista, S. Ntim, P. Manidurai, S. Espinoza, C. Ramanan, R. Cortes-Huerto and M. Sulpizi, *Journal of Physics Condensed Matter*, 2021, **33**,.

29 M. G. Spirin, S. B. Brichkin, E. S. Yushkov and V. F. Razumov, *High Energy Chemistry*, 2020, **54**, 308–315.

30 B. E. Solsona, J. K. Edwards, P. Landon, A. F. Carley, A. Herzing, C. J. Kiely and G. J. Hutchings, *Chemistry of Materials*, 2006, **18**, 2689–2695.

31 F. Calaza, M. Mahapatra, M. Neurock and W. T. Tysoe, *Journal of Catalysis*, 2014, **312**, 37–45.

32 X. Sun, F. Li, Z. Wang, H. An, W. Xue, X. Zhao and Y. Wang, *Chemical Engineering Journal*, 2023, **475**, 146143.

33 D. Astruc, *Chemical Reviews*, 2020, **120**, 461–463.

34 D. Nelli, C. Roncaglia, R. Ferrando and C. Minnai, *The Journal of Physical Chemistry Letters*, 2021, **12**, 4609–4615.

35 C. Fernández-Navarro and S. Mejía-Rosales, *Journal of physical chemistry. C*, 2017, **121**, 21658–21664.

36 R. Cortes-Huerto, J. Goniakowski and C. Noguera, *The Journal of Chemical Physics*, 2013, **138**, 244706.

37 F. Baletto, *LoDis*, 2021, `https://github.com/kcl-tscm/LoDiS`.

38 V. Rosato, M. Guillope and B. Legrand, *Philosophical Magazine A*, 1989, **59**, 321–336.

39 F. Baletto, C. Mottet and R. Ferrando, *Phys. Rev. Lett.*, 2000, **84**, 5544–5547.

40 M. Mariscal, S. Dassie and E. Leiva, *The Journal of chemical physics*, 2005, **123**, 184505.

41 F. Baletto;, R. Ferrando;, A. Fortunelli;, F. Montalenti; and C. Mottet, *J. Chem. Phys.*, 2002, **116**, 3856–3863.

42 D. J. Borbón-González, A. Fortunelli, G. Barcaro, L. Sementa, R. L. Johnston and A. Posada-Amarillas, *The Journal of Physical Chemistry A*, 2013, **117**, 14261–14266.

43 R. Cortes-Huerto, J. Goniakowski and C. Noguera, *Phys. Chem. Chem. Phys.*, 2015, **17**, 6305–6313.

44 M. Jones, Robert, K. Rossi, C. Zeni, M. Vanzan, I. Vasiljevic, A. Santana-Bonilla and F. Baletto, *Faraday Discuss.*, 2023, **242**, 326–352.

45 L. Delgado-Callico, K. Rossi, R. Pinto-Miles, P. Salzbrenner and F. Baletto, *Nanoscale*, 2021, **13**, 1172–1180.

46 H. Abdulhussein, I. Demiroglu and R. Johnston, *The European Physical Journal B*, 2018, **91**,.